

# A convergent blind deconvolution method for post-adaptive-optics astronomical imaging

M Prato<sup>1</sup>, A La Camera<sup>2</sup>, S Bonettini<sup>3</sup> and M Bertero<sup>2</sup>

<sup>1</sup> Dipartimento di Scienze Fisiche, Informatiche e Matematiche, Università di Modena e Reggio Emilia, Via Campi 213/b, 41125 Modena, Italy

<sup>2</sup> Dipartimento di Informatica, Bioingegneria, Robotica e Ingegneria dei Sistemi, Via Dodecaneso 35, 16145 Genova, Italy

<sup>3</sup> Dipartimento di Matematica e Informatica, Università di Ferrara, Via Saragat 1, 44122 Ferrara, Italy

E-mail: marco.prato@unimore.it, andrea.lacamera@unige.it,  
silvia.bonettini@unife.it, bertero@disi.unige.it

**Abstract.** In this paper we propose a blind deconvolution method which applies to data perturbed by Poisson noise. The objective function is a generalized Kullback-Leibler (KL) divergence, depending on both the unknown object and unknown point spread function (PSF), without the addition of regularization terms; constrained minimization, with suitable convex constraints on both unknowns, is considered. The problem is non-convex and we propose to solve it by means of an inexact alternating minimization method, whose global convergence to stationary points of the objective function has been recently proved in a general setting. The method is iterative and each iteration, also called outer iteration, consists of alternating an update of the object and the PSF by means of fixed numbers of iterations, also called inner iterations, of the scaled gradient projection (SGP) method. Therefore the method is similar to other proposed methods based on the Richardson-Lucy (RL) algorithm, with SGP replacing RL. The use of SGP has two advantages: first, it allows to prove global convergence of the blind method; secondly, it allows the introduction of different constraints on the object and the PSF. The specific constraint on the PSF, besides non-negativity and normalization, is an upper bound derived from the so-called Strehl ratio (SR), which is the ratio between the peak value of an aberrated versus a perfect wavefront. Therefore a typical application, but not the unique one, is to the imaging of modern telescopes equipped with adaptive optics systems for partial correction of the aberrations due to atmospheric turbulence. In the paper we describe in detail the algorithm and we recall the results leading to its convergence. Moreover we illustrate its effectiveness by means of numerical experiments whose results indicate that the method, pushed to convergence, is very promising in the reconstruction of non-dense stellar clusters. The case of more complex astronomical targets is also considered, but in this case regularization by early stopping of the outer iterations is required. However the proposed method, based on SGP, allows the generalization to the case of differentiable regularization terms added to the KL divergence, even if this generalization is outside the scope of this paper.

## 1. Introduction

Blind deconvolution is the problem of image deblurring when the blur is unknown and, in general, is investigated by assuming a space-invariant model; in such a case the naive problem formulation is to solve the equation

$$\mathbf{g} = \mathbf{h} * \mathbf{f} \quad ,$$

where  $\mathbf{g}$  is the detected image and  $(\mathbf{f}, \mathbf{h})$  are respectively the unknown object and the unknown point spread function (PSF), while  $*$  denotes convolution. It is obvious that this problem is extremely undetermined and that there is an infinite set of pairs solving the equation. Among them also the trivial solution  $(\mathbf{f} = \mathbf{g}, \mathbf{h} = \boldsymbol{\delta})$ , where  $\boldsymbol{\delta}$  denotes the usual delta function. Therefore the problem must be reformulated by introducing as far as possible all available *a priori* information on both the object and the PSF.

Blind deconvolution is the subject of a wide literature and we do not try to give a thorough account for that. Indeed the different approaches concern specific classes of images and PSFs. For instance approaches applicable to natural images may not be suitable in microscopy; approaches developed for motion blur are not applicable to other classes of blur, and so on. As concerns natural images we only mention a recent paper [32] which contains a critical analysis as well as several relevant references.

In this paper we focus on astronomical imaging by assuming that an adaptive optics (AO) system is used to compensate for atmospheric blur and that a parameter characteristic of this correction, the so-called Strehl ratio (SR), is approximately known. We recall that SR is the ratio of peak diffraction intensity of an aberrated versus perfect waveform. In the case of AO images this parameter can be estimated by the astronomers during the observation and provided with an error of few percent (about 4-5 %). Since this information provides an upper bound on the maximum value of the PSF, it can be used to exclude the trivial solution mentioned above and corresponding to the pair  $(\mathbf{g}, \boldsymbol{\delta})$ .

The approach we propose applies to astronomical imaging if noise is dominated by photon counting and therefore the data are realizations of Poisson processes, even if approaches based on regularized least-square methods are also available (see for instance [29]). In the Poisson case several iterative methods have been already investigated, which consist of alternating updates of the object and PSF by means of Richardson-Lucy (RL) iterations [28, 23, 30, 42, 20, 21], or accelerated RL iterations [10].

In [28] one iteration of the algorithm consists of updating both the object and the PSF by means of one RL iteration. This algorithm was investigated, in a different context, by Lee and Seung [31] but their convergence proof is incomplete, since only the monotonic decrease of the objective function is shown while, for a general descent method to be convergent, strongest Armijo-like decreasing conditions have to be verified [35]. The other approaches could be classified as methods of inexact alternating minimization since they use alternately a number of RL iterations on both the object and the PSF (remark,

however, that the optimization problem underlying these approaches is not explicitly mentioned by the authors). Their convergence is not proved if RL, or the acceleration of RL proposed in [10], are the algorithms used for inexact optimization.

In a recent paper [14], in the context of non-negative matrix factorization, convergence of inexact alternating minimization is proved if the iterative algorithm used for the inner iterations satisfies suitable conditions, which are satisfied by the scaled gradient projection method (SGP) [11] proposed for constrained minimization of convex differentiable functions. Therefore in this paper we utilize these results to propose a convergent blind deconvolution approach applicable to the reconstruction of astronomical adaptive-optics (AO) corrected images. We remark that the advantage of SGP is not only a fast convergence, if a suitable scaling of the gradient is used, but also the possibility of introducing suitable convex constraints on the solution. The practical limitation is that the projection operator onto the convex set defined by the constraints should be easily computable. This is the case of box and equality constraints and the constraints we introduce on the PSF just belong to this class. Remark that, in the case of Gaussian noise, a similar situation is achievable if the projected Landweber method is used (for an application to seismology see [5]) or, more precisely, the accelerated version provided by the application of gradient projection methods [3]. Indeed, in this case the conditions required in [14] for convergence are satisfied.

The structure of our approach is similar to that of the previously mentioned methods based on the RL algorithm, the difference being of course that RL is replaced by SGP with different constraints on  $\mathbf{f}$  and  $\mathbf{h}$ : in the case of the object we only consider non-negativity while in the case of the PSF we consider both non-negativity and an upper bound provided by the knowledge of the SR, as well as the normalization condition which must be satisfied by the PSF. We point out that the relevance of the use of the SR constraint for blind deconvolution was first pointed out by Desiderà & Carbillet [21] and this paper intends to use it in a proper mathematical context.

Thanks to [14] the convergence is assured if we use a fixed number of SGP iterations for updating the object and the PSF; the number of iterations may be different in the two cases (for the denomination *asymmetric iterative blind deconvolution*, see [10]). Since the problem is non-convex, the limit of the iteration may depend on the choice of the initial step and possibly on the numbers of internal iterations. The convergence result does not assure that the limit is a sensible solution of the problem, since we do not introduce regularization in our approach. A comment on this point is required.

In the case of deconvolution it is well known that the minimizers of the discrepancy function for Poisson data, the generalized Kullback-Leibler (KL) divergence, are sparse objects, i.e. they consist of bright spots over a black background; it is the so-called *night-sky* [1] or *checker-board* [34] effect. As a result these minimizers can be sensible solutions in the case, for instance, of the deconvolution of images of not dense star clusters by a

given PSF and this result is confirmed by a wide set of numerical experiments. On the other hand, if the data is the image of a star cluster and we deconvolve it using a sparse object with points correctly located at the positions of the stars, we may expect that the result is a satisfactory reconstruction of the PSF; this reconstruction should improve as the reconstructed image used in the deconvolution improves. Therefore, using a suitable strategy in the choice of the number of inner iterations, we can expect sensible results in the case of stellar objects, by pushing to convergence the outer iterations. This argument is supported by our numerical experiments.

The situation is different in the case of diffuse or complex objects. In this case we can believe that the semi-convergent behaviour of RL or SGP or similar methods implies a similar behaviour for the outer iterations of the blind method; and this is just what we find in our tests. An alternative is obviously the introduction of regularization by adding suitable penalty terms to the KL divergence. However there are two main problems: the first is the selection of a suitable regularization for the astronomical object to be reconstructed and of a suitable regularization for the PSF to be reconstructed; the second is the selection of a suitable rule for estimating the two regularization parameters. We do not know generally accepted solutions for both problems and therefore early stopping of the iterations is still the easiest approach to regularization. We only remark that the proposed method can be easily generalized to the case of differentiable penalties thanks to the generalization of SGP to the regularized case, as proposed in several papers [43, 40, 13].

The paper is organized as follows. In Sect. 2 we formulate the blind deconvolution problem as a constrained minimization of the generalized KL divergence as follows from a maximum-likelihood approach to Poisson data deblurring [6]. In Sect. 3 we summarize the results on the inexact alternating minimization problem proved in [14] as well the main features of the SGP method proposed in [11]. In both cases we also provide the algorithms used in this paper. Finally in Sect. 4 we describe our numerical experiments with a particular focus on the case of astronomical objects consisting of small star clusters, represented in our simulations by point-wise objects. In these cases we observe a remarkable convergence of the reconstructed PSF to that used in image simulations. We also attempt an accurate analysis of the artifacts generated in the reconstructed images since an understanding of their structure may be important in the practical applications of our method. Sect. 5 is devoted to a few conclusions and possible extensions.

## 2. Problem setting

Following [38], we assume that the observed image  $\mathbf{g}$  can be modeled as the sum of two terms  $\mathbf{g} = \mathbf{g}_{pe} + \mathbf{r}$ . The first,  $\mathbf{g}_{pe}$ , is the number of photo-electrons due to object and background emission and is a realization of a Poisson random variable with expected value  $\tilde{\mathbf{g}} = \tilde{\mathbf{h}} * \tilde{\mathbf{f}} + \mathbf{b}$ , where  $\tilde{\mathbf{f}}$  is the original object,  $\tilde{\mathbf{h}}$  is the PSF of the acquisition system and

$\mathbf{b}$  is the background term, while  $\mathbf{r}$  represents the read-out noise (RON). Here and in the following we denote by bold letters  $N \times N$  arrays whose pixels are indexed by a multi-index  $\mathbf{i} = (i_1, i_2)$ ,  $\mathbf{i} \in S$ . For simplicity we assume that the background is constant and known. As concerns the RON, it is a realization of a Gaussian additive random variable with a known variance  $\sigma^2$ . According to Snyder et al. [39], it can be approximated by a Poisson process with mean and variance being the same as  $\sigma^2$  if the constant term  $\sigma^2$  is added to  $\mathbf{g}$ . If we add  $\sigma^2$  also to the background and if, with an abuse of notation, we denote again as  $\mathbf{g}$  and  $\mathbf{b}$  the modified image and background, then we can conclude that

$$\mathbf{g} \sim \text{Poiss}(\tilde{\mathbf{h}} * \tilde{\mathbf{f}} + \mathbf{b}) .$$

As concerns the PSF, we assume that it is normalized to unit volume

$$\sum_{\mathbf{i} \in S} \tilde{\mathbf{h}}_{\mathbf{i}} = 1 \quad (1)$$

and that its maximum value, denoted by  $s$ , is known

$$\max_{\mathbf{i} \in S} \tilde{\mathbf{h}}_{\mathbf{i}} = s. \quad (2)$$

The upper bound  $s$  can be obtained by computing the diffraction-limited PSF of the considered telescope and multiplying its peak value by the SR value provided by the astronomers, as discussed in the Introduction.

The blind deconvolution problem consists in finding an approximation of both  $\tilde{\mathbf{f}}$  and  $\tilde{\mathbf{h}}$ , given  $\mathbf{g}$ ,  $\mathbf{b}$  and  $s$ . To this purpose we consider a maximum-likelihood approach to the problem of image deconvolution. Since the maximization of the likelihood, which depends on the unknown object and PSF, is equivalent to the minimization of a generalized KL divergence, we propose to estimate these approximations by minimizing this function (see the comments in the Introduction concerning regularization) while taking into account all the available information, i.e. the non-negativity of both the PSF and the original object and the constraints (1)-(2). The resulting optimization problem is the following

$$\begin{aligned} \min \quad & KL(\mathbf{g}, \mathbf{h} * \mathbf{f} + \mathbf{b}) \\ \text{s.t.} \quad & \mathbf{f} \geq 0 ; 0 \leq \mathbf{h} \leq s , \sum_{\mathbf{i} \in S} \mathbf{h}_{\mathbf{i}} = 1 \end{aligned} \quad (3)$$

where  $KL$  denotes the KL divergence of  $\mathbf{h} * \mathbf{f} + \mathbf{b}$  from  $\mathbf{g}$

$$KL(\mathbf{g}, \mathbf{h} * \mathbf{f} + \mathbf{b}) = \sum_{\mathbf{i} \in S} \left\{ \mathbf{g}_{\mathbf{i}} \log \frac{\mathbf{g}_{\mathbf{i}}}{(\mathbf{h} * \mathbf{f})_{\mathbf{i}} + \mathbf{b}_{\mathbf{i}}} + (\mathbf{h} * \mathbf{f})_{\mathbf{i}} + \mathbf{b}_{\mathbf{i}} - \mathbf{g}_{\mathbf{i}} \right\} . \quad (4)$$

Problem (3) is convex if restricted to  $\mathbf{f}$  or  $\mathbf{h}$  only, but is in general non-convex with respect to the pair  $(\mathbf{f}, \mathbf{h})$ , thus leading to the possible presence of several local minima.

Indeed, the gradient and Hessian of the objective function in (3) are given by

$$\begin{aligned}\nabla_{\mathbf{f}} KL(\mathbf{g}, \mathbf{h} * \mathbf{f} + \mathbf{b}) &= \mathbf{1} - H^T \frac{\mathbf{g}}{\mathbf{h} * \mathbf{f} + \mathbf{b}} \\ \nabla_{\mathbf{h}} KL(\mathbf{g}, \mathbf{h} * \mathbf{f} + \mathbf{b}) &= F^T \mathbf{1} - F^T \frac{\mathbf{g}}{\mathbf{h} * \mathbf{f} + \mathbf{b}} \\ \nabla^2 KL(\mathbf{g}, \mathbf{h} * \mathbf{f} + \mathbf{b}) &= \\ &\left( \begin{array}{cc} H^T \text{diag} \left( \frac{\mathbf{g}}{(\mathbf{h} * \mathbf{f} + \mathbf{b})^2} \right) H & H^T \text{diag} \left( \frac{\mathbf{g}}{(\mathbf{h} * \mathbf{f} + \mathbf{b})^2} \right) F - K(\mathbf{h}, \mathbf{f}) \\ F^T \text{diag} \left( \frac{\mathbf{g}}{(\mathbf{h} * \mathbf{f} + \mathbf{b})^2} \right) H - K(\mathbf{h}, \mathbf{f})^T & F^T \text{diag} \left( \frac{\mathbf{g}}{(\mathbf{h} * \mathbf{f} + \mathbf{b})^2} \right) F \end{array} \right)\end{aligned}$$

where  $H$  and  $F$  are the Block Circulant with Circulant Blocks (BCCB) matrices associated to the convolution, i.e.  $\mathbf{h} * \mathbf{f} = H\mathbf{f} = F\mathbf{h}$ , while  $K(\mathbf{h}, \mathbf{f})$  is the Block Hankel with Hankel Blocks (BHHB) matrix whose last row is the vector  $\frac{\mathbf{g}}{\mathbf{h} * \mathbf{f} + \mathbf{b}}$  (see [27, Chapter 4] for a survey on structured matrices). Here the ratios and the squares are computed element-wise, and  $\mathbf{1}$  is a column vector with all entries equal to 1. Even if the diagonal blocks of the Hessian are symmetric positive semi-definite, the whole matrix is difficult to analyze and compute.

### 3. Alternating Minimization

Despite the complexity of the Hessian, the constraints have a simple, separable structure, which can be exploited by adopting an Alternating Minimization (AM) algorithm for the solution of the non-convex problem (3)-(4). More precisely, the AM algorithms can be applied to any problem of the form

$$\begin{aligned}\min \quad & J(\mathbf{x}) \\ \text{s.t.} \quad & \mathbf{x} \in \Omega_1 \times \Omega_2 \times \dots \times \Omega_m \subseteq \mathbb{R}^n\end{aligned}\tag{5}$$

where, for all  $i = 1, \dots, m$ ,  $\Omega_i$  is a closed and convex subset of  $\mathbb{R}^{n_i}$  with  $n_1 + \dots + n_m = n$  and any vector in the feasible set can be partitioned into vector components as  $\mathbf{x} = (\mathbf{x}_1, \mathbf{x}_2, \dots, \mathbf{x}_m)$   $\mathbf{x}_i \in \Omega_i$ . Clearly, the blind deconvolution problem (3) is a special case of (5) with  $m = 2$ ,  $\mathbf{x}_1 = \mathbf{f}$  and  $\mathbf{x}_2 = \mathbf{h}$ .

The basic idea of AM is the cyclic minimization of the objective function with respect to one variable, updating its value for the next optimization steps: in particular, AM is often referred to as the *Nonlinear Gauss-Seidel (GS) method*, where the iterate  $\mathbf{x}^{(k+1)} = (\mathbf{x}_1^{(k+1)}, \dots, \mathbf{x}_m^{(k+1)})$  is computed such that for  $i = 1, \dots, m$  the block of variables  $\mathbf{x}_i^{(k+1)}$  is a solution of the sub-problem

$$\begin{aligned}\min \quad & J(\mathbf{x}_1^{(k+1)}, \dots, \mathbf{x}_{i-1}^{(k+1)}, \mathbf{y}, \mathbf{x}_{i+1}^{(k)}, \dots, \mathbf{x}_m^{(k)}) . \\ \text{s.t.} \quad & \mathbf{y} \in \Omega_i\end{aligned}\tag{6}$$

This kind of approach has been widely studied in the literature [8, 9, 25, 26, 33, 41] and we recall two important facts about it:

- for  $m = 2$  it has been proved in [26, Corollary 2] that the limit points of the sequence  $\{\mathbf{x}^{(k)}\}$  defined in (6) are stationary for problem (5) even in the non-convex case;
- for  $m \geq 3$  the convergence of the nonlinear GS method (6) to a solution of (5) is not guaranteed, without additional convexity assumptions on the objective function  $J$ : indeed, in [36], Powell devises a counterexample with  $m = 3$  where all the limit points of the sequence generated by the nonlinear GS method are not stationary for the problem (5). Some convergence results are proved for example in [8, 9, 26, 33] under suitable strict convexity assumptions.

All the convergence results mentioned above, even in the case  $m = 2$ , are proved when the iterates are updated by an *exact* solution of the partial minimization problem (6), which is often impractical or too costly to compute. Indeed, many practical AM algorithms, which are also referred to as *Block Coordinate Descent methods*, are obtained by applying an iterative minimization method to approximately solve (6). In this case, the convergence properties of the alternating scheme also depend on the features of the inner solver. A detailed analysis of the Block Coordinate Descent algorithms in the unconstrained case is proposed in [25], where the authors devise some convergence conditions not necessarily related to the convexity of the objective function.

In this paper, we follow the approach in [14], where the partial minimization over each variable (6) is performed *inexactly* by means of a fixed number of Scaled Gradient Projection (SGP) steps [11].

$$\begin{array}{l}
 \text{Choose a feasible starting point } \mathbf{x}^{(0)} \text{ and a positive integer } L \geq 1 \\
 \text{For } k = 0, 1, 2, \dots \\
 \left[ \begin{array}{l}
 \text{For } i = 1, \dots, m \\
 \left[ \text{Compute } \mathbf{x}_i^{(k+1)} \text{ by applying } n_i^{(k+1)} \leq L \text{ SGP iterations to (6)} \right.
 \end{array} \right.
 \end{array} \tag{7}$$

A representation of the scheme (7) applied to the blind deconvolution problem is given in Algorithm 1: each main cycle consists of two successive deconvolution steps to update the current estimates of the object  $\mathbf{f}^{(k)}$  and PSF  $\mathbf{h}^{(k)}$ . For sake of completeness, we report the convergence result shown in Theorem 4.2 of [14] for our particular case.

**Theorem 3.1** *Every limit point of the sequence  $(\mathbf{f}^{(k)}, \mathbf{h}^{(k)})$  generated by Algorithm 1 is a stationary point for problem (3).*

As far as we know, convergence results stronger than that given in this Theorem for first-order methods applied to a general non-convex problem do not exist in the literature. The main difficulty in this kind of problems is to prove the existence of convergent subsequences. However, in our specific case, thanks to the Strehl constraint, the sequence of the PSFs generated by our approach is bounded. Moreover, as concerns object reconstruction one could introduce a constraint on the flux ( $\ell_1$  norm) of the reconstructed

objects since this parameter can be derived from the data. However, as follows from our numerical experience this constraint is practically assured by SGP (we recall that it is exactly assured by RL in the case of zero background) and therefore we do not introduce it in order to reduce the computational cost. It follows that also the sequence of the reconstructed objects is bounded. We conclude that the existence of convergent sub-sequences is assured. We can add that we remarked a convergent behaviour of all the sequences obtained in our numerical experiments.

Finally, we point out that the convergence result holds for any number of inner SGP iterations. The key point of such theoretical analysis is the sufficient decrease of the objective function, which is enforced at each SGP iteration by means of an Armijo backtracking loop. Since the objective function (4) is not convex with respect to the couple  $(\mathbf{f}, \mathbf{h})$ , the presence of multiple potential stationary points makes any limit point dependent on both the initial guess and the chosen inner iteration numbers on the image  $(n_f)$  and the PSF  $(n_h)$ .

---

**Algorithm 1** Cyclic Scaled Gradient Projection (CSGP) method

---

Choose the starting point  $\mathbf{f}^{(0)}, \mathbf{h}^{(0)}$  and the inner iterations numbers  $n_f, n_h \geq 1$ .

FOR  $k = 0, 1, 2, \dots$  DO THE FOLLOWING STEPS:

STEP 1. Compute  $\mathbf{f}^{(k+1)}$  with  $n_f$  SGP iterations applied to

$$\min KL(\mathbf{g}, \mathbf{h}^{(k)} * \mathbf{f} + \mathbf{b}) \quad (8)$$

$$\text{s.t. } \mathbf{f} \geq 0$$

starting from the point  $\mathbf{f}^{(k)}$

STEP 2. Compute  $\mathbf{h}^{(k+1)}$  with  $n_h$  SGP iterations applied to

$$\min KL(\mathbf{g}, \mathbf{h} * \mathbf{f}^{(k+1)} + \mathbf{b}) \quad (9)$$

$$\text{s.t. } 0 \leq \mathbf{h} \leq s, \sum_{i \in S} \mathbf{h}_i = 1$$

starting from the point  $\mathbf{h}^{(k)}$ .

END

---

We stress the fact that the main strength of Algorithm 1 for blind deconvolution with respect to the more standard AM approach described for example in [16], is that it allows an inexact solution of the inner sub-problems (8)–(9) while preserving the theoretical convergence properties. Since the proposed method is essentially based on SGP, we recall its main features in the following sub-section.

### 3.1. The Scaled Gradient Projection method

The SGP algorithm is a first-order method which applies to any optimization problem of the form

$$\min_{\mathbf{x} \in \Omega} J(\mathbf{x}) \quad (10)$$

where  $J(x)$  is a continuously differentiable function and  $\Omega$  is a convex set. Each SGP iteration is based on the feasible descent direction defined as

$$\mathbf{d}^{(k)} = P_{\Omega, D_k^{-1}}(\mathbf{x}^{(k)} - \alpha_k D_k \nabla J(\mathbf{x}^{(k)})) - \mathbf{x}^{(k)}$$

where  $\alpha_k$  is a scalar step-size parameter,  $D_k$  is a diagonal matrix with positive diagonal entries and  $P_{\Omega, D_k^{-1}}(\cdot)$  is the projection onto  $\Omega$  associated to the norm induced by  $D_k^{-1}$ , i.e.

$$P_{\Omega, D_k^{-1}}(\mathbf{x}) = \arg \min_{\mathbf{y} \in \Omega} (\mathbf{x} - \mathbf{y})^T D_k^{-1} (\mathbf{x} - \mathbf{y}). \quad (11)$$

The new point is computed along the direction  $\mathbf{d}^{(k)}$  as follows

$$\mathbf{x}^{(k+1)} = \mathbf{x}^{(k)} + \lambda_k \mathbf{d}^{(k)}$$

where  $\lambda_k$  is a step-length parameter to be chosen such that the monotone Armijo condition

$$J(\mathbf{x}^{(k)} + \lambda_k \mathbf{d}^{(k)}) \leq J(\mathbf{x}^{(k)}) + \beta \lambda_k \nabla J(\mathbf{x}^{(k)})^T \mathbf{d}^{(k)} \quad (12)$$

is satisfied for a fixed value of the parameter  $\beta \in (0, 1)$ , in order to guarantee the sufficient decrease of the objective function. In practice,  $\lambda_k$  is computed by a standard backtracking condition as  $\lambda_k = \theta^m$ , where  $\theta \in (0, 1)$  and  $m$  is the smallest integer such that (12) is satisfied.

The convergence of the SGP scheme, which is outlined in Algorithm 2, can be proved when the step-size  $\alpha_k$  and the diagonal entries of  $D_k$  are bounded above and away from zero, i.e.  $\alpha_k \in [\alpha_{min}, \alpha_{max}]$  with  $0 < \alpha_{min} < \alpha_{max}$  and  $D_k$  is chosen in the set  $\mathcal{D}$  of diagonal matrices whose diagonal entries have values between  $L_1$  and  $L_2$ , for given thresholds  $0 < L_1 < L_2$ .

The SGP algorithm has been recently applied in several image restoration problems (see e.g. [3, 12, 43]). Under standard assumptions, it can be proved [11] that the SGP algorithm is well defined and any limit point of the sequence  $\{\mathbf{x}^{(k)}\}$  is a stationary point of (10); if, in addition,  $J(\mathbf{x})$  is convex, any limit point is a minimum point. It is worth stressing that the convergence result holds for any choice of the scaling matrix  $D_k \in \mathcal{D}$  and the step-length  $\alpha_k \in [\alpha_{min}, \alpha_{max}]$ : this freedom of choice can be exploited in order to improve the convergence speed. Indeed, it is well known that gradient methods can be significantly accelerated by a clever choice of the step-length parameter  $\alpha_k$ : one of the more effective strategies are the Barzilai–Borwein (BB) rules proposed firstly in [2] for quadratic unconstrained programming and then developed and analyzed for more general problems (see [17, 19, 24, 44] and reference therein). The BB rules can be considered a very

**Algorithm 2** Scaled gradient projection (SGP) method

Choose the starting point  $\mathbf{x}^{(0)} \geq 0$  and set the parameters  $\beta, \theta \in (0, 1)$ ,  $0 < \alpha_{min} < \alpha_{max}$ .

FOR  $k = 0, 1, 2, \dots$  DO THE FOLLOWING STEPS:

STEP 1. Choose the parameter  $\alpha_k \in [\alpha_{min}, \alpha_{max}]$  and the scaling matrix  $D_k \in \mathcal{D}$ ;

STEP 2. Compute the descent direction:

$$\mathbf{d}^{(k)} = P_{\Omega, D_k^{-1}}(\mathbf{x}^{(k)} - \alpha_k D_k \nabla J(\mathbf{x}^{(k)})) - \mathbf{x}^{(k)};$$

STEP 3. Backtracking loop: compute the smallest integer  $m$  such that (12) is satisfied with  $\lambda_k = \theta^m$ ;

STEP 4. Set  $\mathbf{x}^{(k+1)} = \mathbf{x}^{(k)} + \lambda_k \mathbf{d}^{(k)}$ .

END

cheap way to capture the second order information enforcing a quasi-Newton property. In our algorithm we adopt the scaled versions of the BB rules proposed in [11], which are given by

$$\alpha_k^{(BB1)} = \frac{\mathbf{s}^{(k-1)T} D_k^{-1} D_k^{-1} \mathbf{s}^{(k-1)}}{\mathbf{s}^{(k-1)T} D_k^{-1} \mathbf{z}^{(k-1)}}, \quad \alpha_k^{(BB2)} = \frac{\mathbf{s}^{(k-1)T} D_k \mathbf{z}^{(k-1)}}{\mathbf{z}^{(k-1)T} D_k D_k \mathbf{z}^{(k-1)}}, \quad (13)$$

where  $\mathbf{s}^{(k-1)} = \mathbf{x}^{(k)} - \mathbf{x}^{(k-1)}$  and  $\mathbf{z}^{(k-1)} = \nabla J(\mathbf{x}^{(k)}) - \nabla J(\mathbf{x}^{(k-1)})$ . Based on the previous formulas, we define the values  $\alpha_k^{(1)}, \alpha_k^{(2)} \in [\alpha_{min}, \alpha_{max}]$  in the following way

IF  $\mathbf{s}^{(k-1)T} D_k^{-1} \mathbf{z}^{(k-1)} \leq 0$  THEN

$$\alpha_k^{(1)} = \min \{10 \cdot \alpha_{k-1}, \alpha_{max}\};$$

ELSE

$$\alpha_k^{(1)} = \min \left\{ \alpha_{max}, \max \left\{ \alpha_{min}, \alpha_k^{(BB1)} \right\} \right\};$$

ENDIF

IF  $\mathbf{s}^{(k-1)T} D_k \mathbf{z}^{(k-1)} \leq 0$  THEN

$$\alpha_k^{(2)} = \min \{10 \cdot \alpha_{k-1}, \alpha_{max}\};$$

ELSE

$$\alpha_k^{(2)} = \min \left\{ \alpha_{max}, \max \left\{ \alpha_{min}, \alpha_k^{(BB2)} \right\} \right\};$$

ENDIF

From the numerical experience, the best performances are obtained by an alternation of the two BB formulas: thus, following [24], we choose the following criterion for computing  $\alpha_k$

IF  $k \leq 20$  THEN

$$\alpha_k = \min_{j=\max\{1, k+1-M_\alpha\}, \dots, k} \alpha_j^{(2)}; \quad (14)$$

ELSE IF  $\alpha_k^{(2)} / \alpha_k^{(1)} \leq \tau_k$  THEN

Set  $\alpha_k$  as in (14)

```

 $\tau_{k+1} = 0.9 \cdot \tau_k;$ 
ELSE
 $\alpha_k = \alpha_k^{(1)}; \quad \tau_{k+1} = 1.1 \cdot \tau_k;$ 
ENDIF

```

where  $M_\alpha$  is a prefixed positive integer and  $\tau_1 \in (0, 1)$ . Our choice of taking the value defined in (14) for the first 20 iterations leads to a more stable behaviour and, in some cases, also to a slight improvement of the reconstruction accuracy [37].

The other crucial ingredient for the practical performances of SGP is the choice of the scaling matrix: in our case, taking into account the objective functions of (8) and (9), we adopt the scaling suggested by the RL algorithm

$$D_k = \text{diag}(\min(L_2, \max(L_1, \mathbf{x}^{(k)})))$$

as suggested also in [11]. Obviously, in the inner iterations of (8),  $\mathbf{x}$  is replaced by  $\mathbf{f}$  while, in the inner iterations of (9),  $\mathbf{x}$  is replaced by  $\mathbf{h}$ . As concerns the choice of the bounds  $(L_1, L_2)$ , at the beginning of each inner subproblem we perform one step of the RL method and tune the parameters according to the min/max positive values  $y_{\min}/y_{\max}$  of the resulting image according to the rule

```

IF  $y_{\max}/y_{\min} < 50$  THEN
 $L_1 = y_{\min}/10;$ 
 $L_2 = y_{\max} \cdot 10;$ 
ELSE
 $L_1 = y_{\min};$ 
 $L_2 = y_{\max};$ 
ENDIF

```

### 3.2. Computing the projections

Since the minimization steps (8) and (9) involve different constraints, corresponding to two convex sets  $\Omega_1$  and  $\Omega_2$ , respectively, we have to account for two different algorithms to compute the projections  $P_{\Omega_1, D_k^{-1}}$  and  $P_{\Omega_2, D_k^{-1}}$ . In the alternating procedure of Algorithm 1, when SGP is applied to problem (8), the projection consists of a simple component thresholding, obtained by setting all the negative elements of the vector to be projected equal to zero. For the updating of the PSF, instead, we have to project on the constraints set of the problem (9), consisting of a single linear equality constraint, in addition to simple bounds (box constraints) on the variables. The resulting constrained optimization problem to be addressed is therefore

$$\begin{aligned}
& \min \quad \frac{1}{2} \mathbf{z}^T D_k^{-1} \mathbf{z} - \mathbf{z}^T \mathbf{y} \\
& \text{s.t.} \quad 0 \leq \mathbf{z} \leq s, \quad \sum_{i \in S} z_i = 1
\end{aligned} \tag{15}$$

where  $\mathbf{y} = D_k^{-1}(\mathbf{x}^{(k)} - \alpha_k D_k \nabla J(\mathbf{x}^{(k)}))$ . By introducing the Lagrangian penalty function, one can see that the orthogonal projection (15) can be re-conducted to a root-finding problem of the piecewise linear monotonically non-decreasing function

$$t(\xi) = \sum_{i \in S} \mathbf{z}_i(\xi) - 1 = 0,$$

where  $\xi$  is the Lagrangian multiplier of the equality constraint,

$$\mathbf{z}_i(\xi) = \text{mid}(0, (D_k)_{ii}(\mathbf{y}_i + \xi), s)$$

and  $\text{mid}(a_1, a_2, a_3)$  is the component-wise operation that supplies the median of its three arguments. For solving this kind of problem we apply the secant-based method proposed in [18] (its Matlab implementation is given in the corresponding technical report downloadable at the webpage [http://www.maths.dundee.ac.uk/nasc/na-reports/NA216\\_RF.pdf](http://www.maths.dundee.ac.uk/nasc/na-reports/NA216_RF.pdf)), which is able to compute the projection very quickly and whose computational cost grows linearly in time with respect to the image size [11, §3.1].

#### 4. Numerical experiments

In this section we investigate the effectiveness of the proposed blind method by means of several numerical experiments. Since the blind problem formulated in (3) is non-convex, several local minima may exist. Moreover, we know that any limit point (or the limit) of the proposed iteration is a stationary point of the problem. The limit depends, in general, on the numbers of inner iterations but also on the initialization of the outer iteration; therefore it is important to initialize the procedure with a sensible initial guess and we first discuss this point.

As concerns the object we can use the standard initialization of the RL algorithm, namely a constant object with a flux coinciding with the flux of the image after background subtraction. The choice of the initial PSF is more important because, in the first step of the procedure, the image is deconvolved with this PSF.

To this purpose we point out an important property of the PSF of a telescope: it is a band-limited function and, if the telescope consists of a circular mirror, the band, i.e. the support of its Fourier transform, is a disc with a radius proportional to the ratio between the diameter  $D$  of the telescope and the observation wavelength  $\lambda$ . It is not easy to insert this property as a constraint on the PSF because the projection on the resulting set of constraints (including SR and normalization) is not easily computable. For this reason we do not consider this constraint in this paper. However we can try to force the estimated PSF to have this property using an initial PSF which is band-limited and satisfies the other constraints.

The ideal PSF of the telescope is not suitable as initial guess because it does not satisfy the SR constraint. However one can consider, as suggested for instance in [10],

the autocorrelation of the ideal PSF, which has the same band. In our simulations, which assume in general a telescope of the 8m class and observations in H-band (see the beginning of the next section), the resolution, inversely proportional to the bandwidth, is about 50 mas (milliarcseconds). Using an oversampling such that the pixel size is 15 mas, the diameter of the band in Fourier space is about 186 pixels (remark that it depends also on the number of pixels in the image). With these values, the autocorrelation is a good choice if  $SR \geq 0.46$  (the value of  $s$  depends on both SR and the ratio  $D/\lambda$ ); for lower values of SR one can take the autocorrelation of the autocorrelation and so on, until the SR constraint is satisfied. This is the choice considered in our numerical experiments and, quite surprisingly, it seems that the algorithm, in spite of its high nonlinearity, preserves the band-limiting property satisfied by the initial guess.

All the numerical experiments have been performed with a set of routines implemented by ourselves in Interactive Data Language (IDL). The codes of the algorithms presented and discussed in this paper are available under request.

#### 4.1. Image generation

As mentioned in the Introduction the use of SR as a constraint on the PSF is first proposed in [21]. Therefore some of our numerical experiments coincide with some of the tests performed in that paper. In particular we use three of the AO-corrected PSFs (with SR equal to 0.67, 0.40 and 0.17, respectively), used by these authors and obtained by means of the Software Package CAOS [15]; the parameters corresponding to these PSFs are given in [21]. We only specify that they correspond to a telescope with an effective diameter of 8.22 m and an observation wavelength of  $\lambda = 1.65\mu\text{m}$  (H-band). For each PSF, the images are generated by assuming, as in [21] a time exposure of 1200 s, with a total transmission of 0.3. Moreover, a background of 13.5 mag arcsec<sup>-2</sup>, corresponding to observations in H-band, is added to the blurred images (for the convenience of the reader we remark that it corresponds to  $3.41 \times 10^4$  counts per pixel). The results are perturbed with Poisson noise and additive Gaussian noise with  $\sigma = 10 e^-/\text{px}$ . According to the approach proposed in [39] and discussed in Sect. 2, RON compensation is obtained in the deconvolution algorithms by adding the constant  $\sigma^2 = 100$  to the images and the background.

In our first experiment we also consider an example which is not related to AO imaging but is a simulation of HST image before COSTAR correction, since this image is frequently used in the testing of deconvolution methods. Obviously in such a case the ideal PSF must be computed, by taking into account the diameter of the Hubble telescope, about 2.4 m, and the assumed observation wavelength of about  $0.55 \mu\text{m}$ , and compared to the aberrated PSF in order to estimate the corresponding SR. Objects, PSFs and blurred images used in all our experiments are sized  $256 \times 256$  pixels.

#### 4.2. Point-wise objects

We first report results on the following examples:

- the binary system considered by Desiderà & Carillet [21], in which the two components have the same magnitude 12 in H-band (corresponding approximately to  $6.03 \times 10^8$  counts) with an angular separation of 285 mas (19 pixels), i.e.  $\sim 7$  times larger than the diffraction limit ( $\sim 40$  mas);
- a model of an open star cluster based on an image of the Pleiades, consisting of 9 stars with magnitudes ranging from about 13 (i.e. about  $2.32 \times 10^8$  counts) to 16 (about  $1.79 \times 10^7$  counts) in H-band and described in [7];
- a simulation of a star cluster, consisting of 470 light sources, as observed by the Hubble Space Telescope (HST) before COSTAR correction. For this case only, we do not use an AO-corrected PSF but the aberrated HST PSF, which corresponds to  $SR=0.09$ . These data can be obtained via anonymous ftp from [ftp://ftp.stsci.edu/software/stsdas/testdata/restore/sims/star\\_cluster/](ftp://ftp.stsci.edu/software/stsdas/testdata/restore/sims/star_cluster/).

In Fig. 1 we show the images of the binary and of the star cluster in the case of a PSF with  $SR=0.67$  as well as the HST image of a simulated star cluster. For all these examples we use 50 inner iterations on the object and 1 inner iteration for the PSF. This choice can be justified by the features of our blind problem discussed in the Introduction, since we need a sufficiently large number of SGP inner iterations for obtaining a nearly point-wise object. Moreover, with a few experiments on the binary, we verify that this choice is a good compromise which provides a sufficiently fast convergence for all cases. In a first instance we perform 300 outer iterations.

As concerns the measure of the quality of the reconstructions, for the PSFs we use the relative r.m.s. error between the reconstructed PSF  $\mathbf{h}$  and that used for image generation  $\tilde{\mathbf{h}}$ , i.e.

$$RMSE = \frac{\|\mathbf{h} - \tilde{\mathbf{h}}\|_2}{\|\tilde{\mathbf{h}}\|_2}, \quad (16)$$

where  $\|\cdot\|_2$  denotes the  $\ell_2$  norm. The same parameter is used for measuring the quality of the reconstruction of the HST star cluster. In the case of the binary and of the open star cluster we use a *magnitude average relative error* (MARE) defined as follows

$$MARE = \frac{1}{q} \sum_{i=1}^q \frac{|m_i - \tilde{m}_i|}{\tilde{m}_i}, \quad (17)$$

where  $q$  is the number of stars and  $m_i$ ,  $\tilde{m}_i$  are respectively the reconstructed and the true magnitudes.

The results are shown in Table 1 and are consistent with the results reported in [21] but obtained with a sound mathematical approach, allowing investigation of the limit

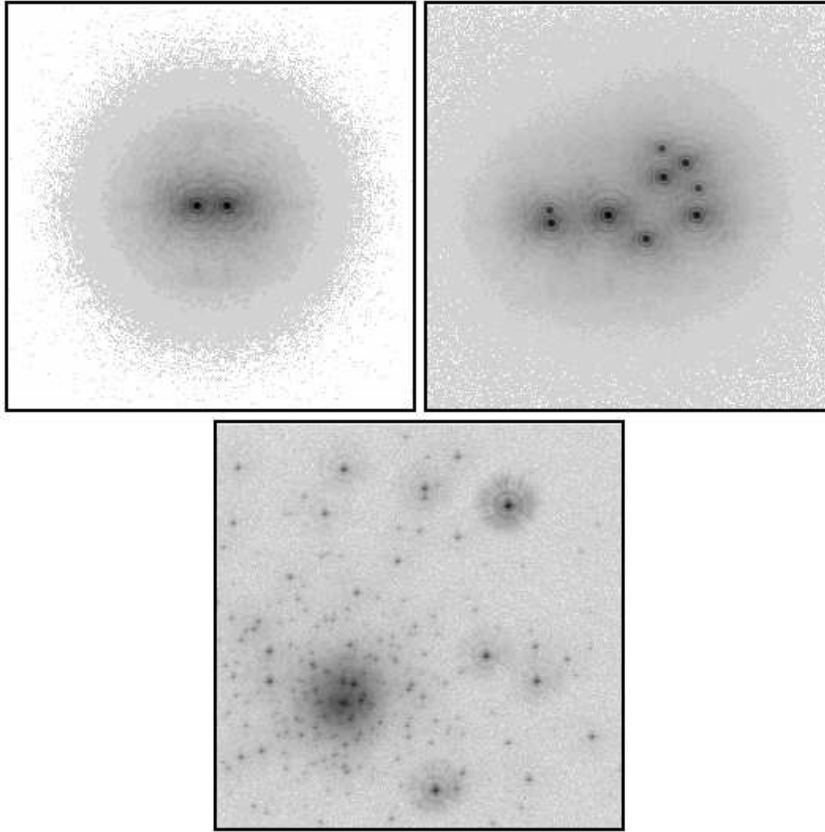


**Figure 1.** Images of the binary and of the star cluster (upper panels) in the case of a PSF with  $SR=0.67$ . In the lower panel the image of the HST star cluster.

for large number of iterations and generalization to regularized problems. The values of MARE estimated with our blind approach are certainly higher than those achievable if one deconvolves the data with the exact PSF (*inverse crime*) and given in the third column, but they are still quite small. Moreover the reconstruction of the PSFs is very satisfactory: the RMSEs of the initial PSFs are of the order of 30-50 %, while those of the reconstructed PSFs are of the order of few percents. A comparison between the true, initial and reconstructed PSFs is shown in Fig. 2. We must add that the reconstruction error is still decreasing after 300 iterations and therefore the minimum of the objective function is not yet reached.

For investigating the limit of the algorithm we consider three other examples of binaries: a binary with magnitudes 12-12 and angular distance of 10 pixels and two binaries with magnitudes 12-16 and angular distances of 19 and 10 pixels respectively. For these four examples of binaries we generate images using the PSF with the highest SR, namely 0.67, and we compute 8000 outer iterations of the blind algorithm, using the fixed pair  $(n_f, n_h) = (50, 1)$ . In Table 2 we report the results obtained after 300,

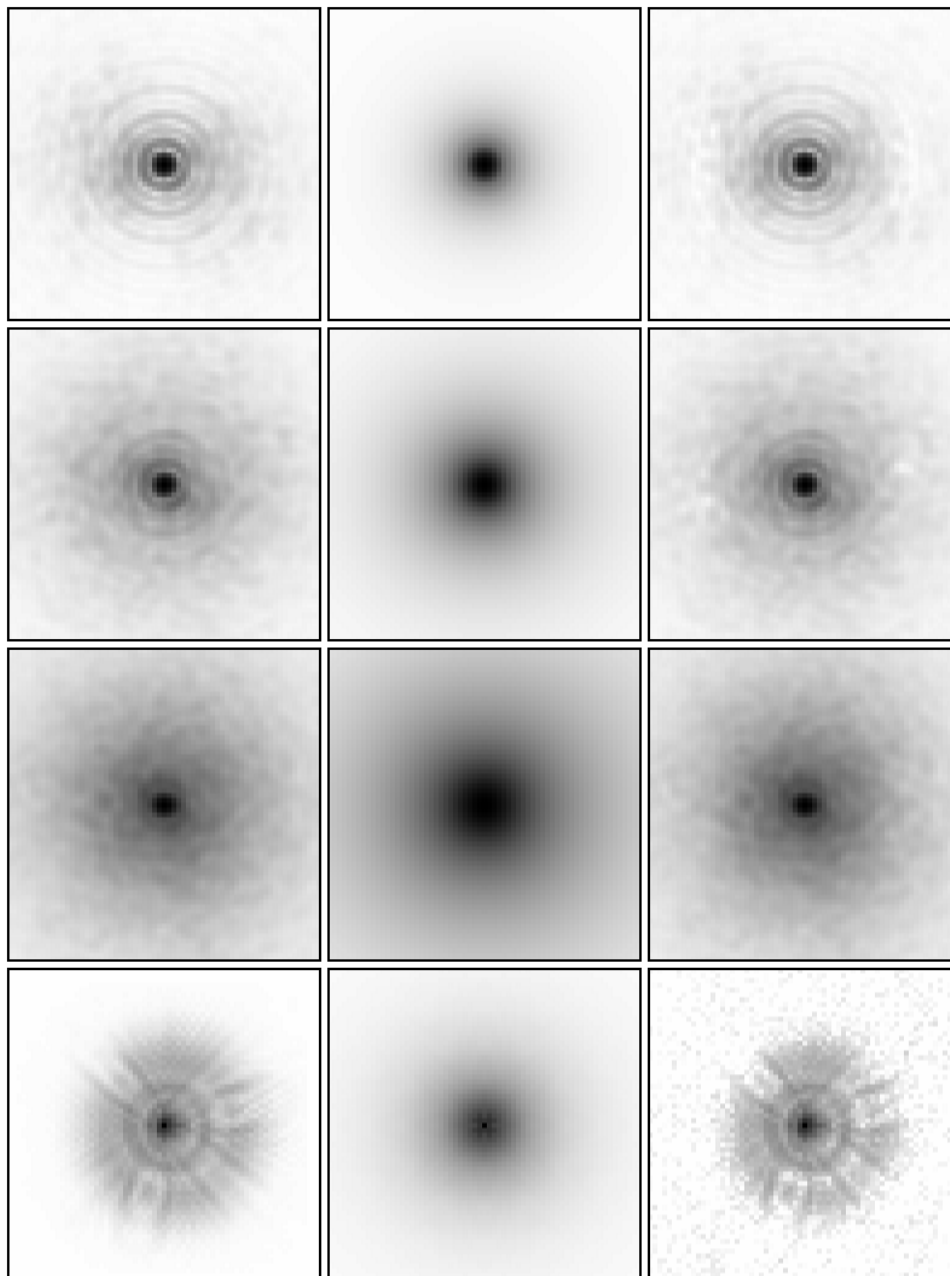


**Figure 2.** First column: the PSFs used for image generation; second column: the PSFs used for initializing the blind algorithm (see the text for their computation); third column: the PSFs reconstructed by the blind algorithm. First row: AO-corrected PSF with  $SR=0.67$ ; second row: AO-corrected PSF with  $SR=0.40$ ; third row: AO-corrected PSF with  $SR=0.17$ ; fourth row: HST PSF before COSTAR correction.

**Table 1.** Reconstruction errors for point-wise objects. In the first column we specify the object and in the second the value of the SR used for image generation; in the third and fourth the values of MARE (RMSE in the case of HST cluster) when SGP is used for image deconvolution with the exact and initial PSF respectively. In the fifth column the values of MARE (RMSE in the case of HST) obtained with 300 outer iterations by our blind approach, using the fixed pair  $(n_f, n_h) = (50, 1)$ . Finally, in the last two columns the errors between the true and the initial PSF, followed by the errors between the true PSF and that provided by the blind approach.

Image	SR	$MARE$	$MARE_1$	$MARE_2$	$RMSE_1$	$RMSE_2$
Binary	0.67	$1.86 \times 10^{-5}$	$1.12 \times 10^{-2}$	$1.44 \times 10^{-3}$	32 %	1.8 %
	0.40	$1.84 \times 10^{-5}$	$2.26 \times 10^{-2}$	$2.15 \times 10^{-3}$	54 %	2.9 %
	0.17	$2.36 \times 10^{-6}$	$1.67 \times 10^{-2}$	$1.99 \times 10^{-3}$	55 %	3.3 %
Cluster	0.67	$2.10 \times 10^{-5}$	$1.07 \times 10^{-2}$	$3.09 \times 10^{-4}$	32 %	1.0 %
	0.40	$4.43 \times 10^{-5}$	$1.14 \times 10^{-2}$	$3.63 \times 10^{-4}$	54 %	1.1 %
	0.17	$5.42 \times 10^{-5}$	$1.30 \times 10^{-1}$	$2.87 \times 10^{-3}$	55 %	4.2 %
HST	0.09	5.1 %	25 %	7.6 %	47 %	6.7 %

4000 and 8000 outer iterations. We do not find a uniform behaviour: in some cases the errors are decreasing for increasing number of iterations while in others they are slightly increasing or do not have a monotone behaviour. In all cases the variations are small and the reconstruction errors on the PSF after 8000 iterations are quite small. However, in view of obtaining a sufficient accuracy, 300 outer iterations can be sufficient in all cases.

Similar results are obtained in the case of the open star cluster. Moreover, since the previous examples are derived from the examples considered in [21] and generated by assuming a very long observation time (hence a low noise level) we also generated an image of the binary 12-12, angular distance 19 pixels, assuming an integration time of 12 seconds, with a reduction by a factor 100 of the average number of photons. By performing 8000 iterations we still find convergence of the algorithm but the error on the PSF is now of the order of 1 % and can be reached after 300 iterations. On the other hand the value of MARE is quite satisfactory since it is of the order of  $8 \times 10^{-4}$ .

It should be interesting to find a way for establishing if the minima we find are the global ones or not, but, as it is known, global minimization is a very difficult problem. As a test, even if it does not provide a proof that the minima are the global ones, we compare the minimum values of the objective function, i.e. the KL divergence, with its values corresponding to the ground truths, i.e. the values obtained by substituting in Eq. (4) the objects and PSFs used for image generation. We find that the minimum values are of the order of  $1.0 \times 10^4$  while the values corresponding to the ground truth are greater by about a factor of 3. We can only say that, if these values were smaller than our minimum

**Table 2.** Reconstruction errors, provided by increasing number of iterations, in the case of four different binaries (the parameters are indicated in the first column, as explained in the text) whose images are generated using the PSF with SR=0.67. As usual MARE is a measure of the errors on the magnitudes of the two stars while RMSE is a measure of the error on the reconstructed PSF.

		300 it	4000 it	8000 it
12-12 19 pixels	MARE	$1.44 \times 10^{-3}$	$1.38 \times 10^{-4}$	$1.31 \times 10^{-4}$
	RMSE	1.8 %	0.17 %	0.15 %
12-16 19 pixels	MARE	$5.10 \times 10^{-4}$	$1.01 \times 10^{-3}$	$1.52 \times 10^{-3}$
	RMSE	0.99 %	0.20 %	0.27 %
12-12 10 pixels	MARE	$1.26 \times 10^{-3}$	$1.42 \times 10^{-4}$	$1.34 \times 10^{-4}$
	RMSE	1.7 %	0.18 %	0.17 %
12-16 10 pixels	MARE	$1.31 \times 10^{-2}$	$1.92 \times 10^{-2}$	$2.22 \times 10^{-2}$
	RMSE	1.1 %	1.3 %	1.5 %

values, then our minima were certainly local.

Before considering other examples it is important to remark that, in the case of the binary and of the small star cluster, the stars are reconstructed as single pixels with a sufficiently accurate flux value, but the reconstructed images contain artifacts, in the sense that other pixels take non zero values. These values are small but they can be disturbing in the case of an accurate photometric analysis, for instance of a star cluster, because they could be detected as faint stars. Indeed the difference of magnitude between the brightest artifact and the true stars is of the order of  $\Delta m = 8$ . For this reason we perform an analysis of this problem in the case of the binary, using the PSF with the highest SR, namely SR=0.67.

#### 4.3. Artifacts analysis

We first consider the inverse crime reconstruction of the binary with magnitudes 12-12 and angular distance 19 pixels. We deconvolve its image generated by means of the PSF with SR=0.67 using the same PSF (inverse crime). The algorithm is the standard SGP with non-negativity constraint. Also in this case the reconstruction is not free of artifacts but they are randomly distributed and their values are quite small: the brightest artifact has a magnitude  $m = 24$ , hence with a difference  $\Delta m = 12$  with respect to the stars of the binary.

Next we apply the blind algorithm, using as a constraint the exact value of SR and we analyze the results provided by the 8000 outer iterations already considered in the previous section. In the first two rows of Fig. 3 we show the reconstructed PSF and the

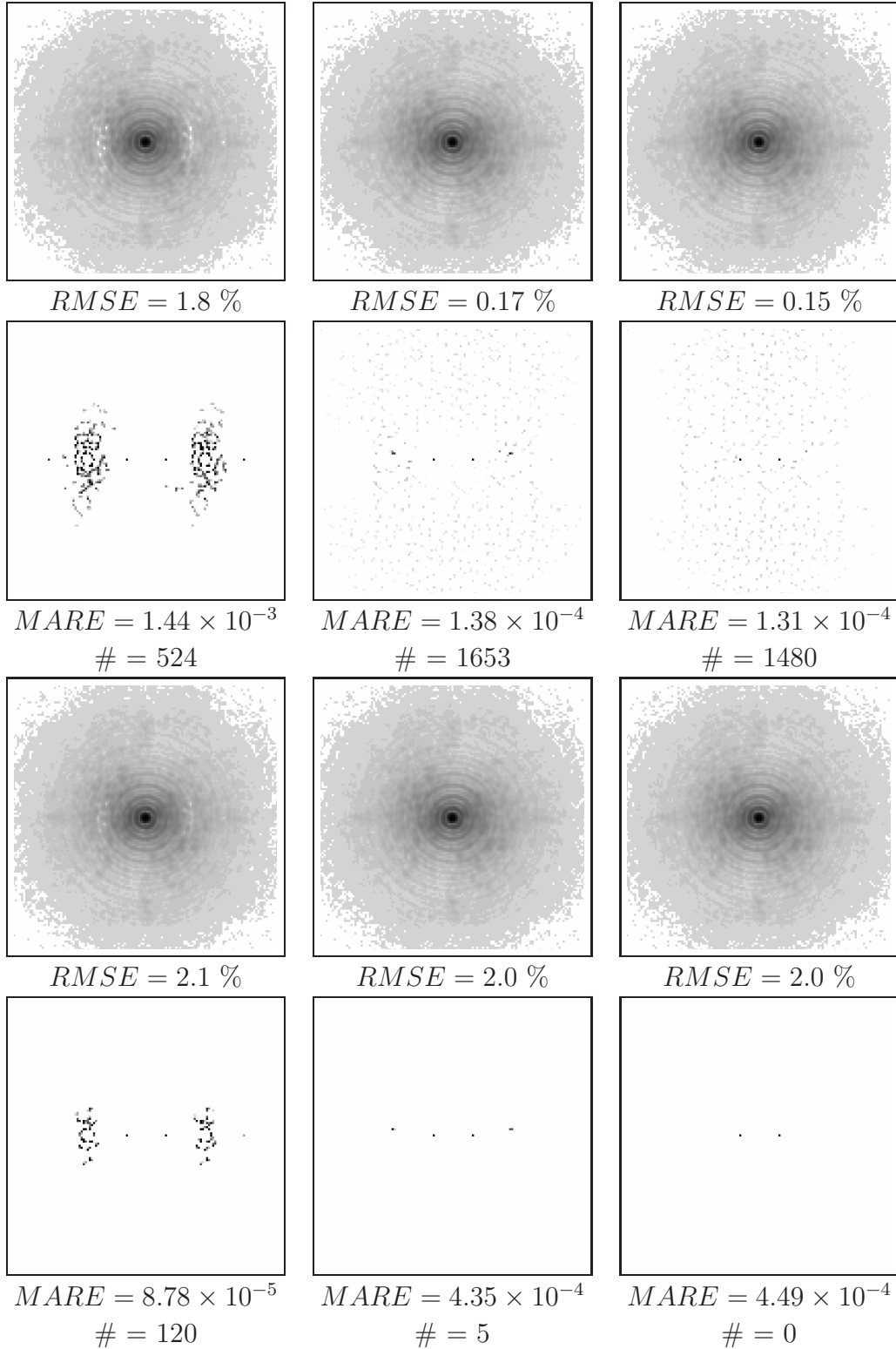


**Figure 3.** Binary with magnitudes 12-12 and angular separation of 19 pixels. First and second row: the reconstructed PSF and object after 300 (left), 4000 (middle), and 8000 (right) outer iterations with the exact value of SR ( $SR=0.67$ ) as a constraint. Third and fourth rows: the reconstructed PSF and object after 300 (left), 500 (middle), and 2000 (right) outer iterations with the underestimated value of SR ( $SR=0.64$ ) as a constraint. The symbol # denotes the number of artifacts.

reconstructed object after 300, 4000 and 8000 outer iterations. The object is represented using a logarithmic and gray-level reversed scale for stressing the artifacts. After 300 iterations a few artifacts appear in the reconstructed PSF in a region corresponding to the positions of the two stars. Therefore, even if the reconstruction error is small, it is evident that it may be convenient to use a larger number of iterations. After 4000 iterations the PSF artifacts disappear and the reconstruction error is really very small, of the order of 0.2%. The situation does not significantly change if we further increase the number of iterations.

As concerns the reconstructed binary, after 300 iterations the artifacts are concentrated along two arcs positioned around the two stars. We checked that this behaviour is stable if we change the noise realization. Again, if we increase the number of iterations the results are better, in the sense that the artifacts are more randomly distributed and the intensity of the brightest one decreases. Indeed, after 4000 iterations we have  $\Delta m = 10$  and after 8000 iterations  $\Delta m = 11$ . We find similar results in the case of the open star cluster and therefore we can conclude that a very large number of iterations may be required for obtaining very good results, at least if the exact value of SR is known.

However, as briefly discussed in the Introduction, it is not possible to know exactly the value of SR. According to astronomers the expected error is of the order of 4 %. Therefore, we consider a variation of the constraint of this order of magnitude for images generated in the case of SR=0.67; more precisely we consider two values, SR=0.7 and SR=0.64. We apply the blind algorithm using as a constraint the corresponding values of  $s$ . In the first case the reconstructions are definitely worse, the number of artifacts considerably increases as well as the error on the PSF. For instance, in the case 12-12 the RMSE is of the order of 5 % and does not decrease with increasing number of iterations (remember that, in the case of exact value, the error after 8000 iterations is of the order of 0.15 %). On the other hand, if we underestimate the SR, i.e. we take as a constraint the value of  $s$  corresponding to SR=0.64, then the results are satisfactory. The reconstruction errors for the four binaries already considered in the previous subsection are reported in Table 3. By comparing with the results reported in Table 2 and referring to the exact constraint, we can conclude that the reconstruction errors are not significantly greater than those obtained in the exact case and that the convergence is faster.

In the case of the binary with magnitudes 12-12 and angular distance 19 pixels we show the reconstructions of the PSF and of the binary after 300, 500 and 2000 iterations respectively in the third and fourth row of Fig. 3. Quite surprisingly, the artifacts in the reconstruction of the binary completely disappear after 2000 iterations and the error on the reconstructed PSF is of the order of 2 %. We can add that the same result is obtained in the case of the open star cluster.

In order to further investigate the effect of a wrong value of  $s$ , in the case of the

**Table 3.** Reconstruction errors in the case of the four different binaries of Table 2 (described in the text), considering an underestimated constraint of the blind algorithm (SR=0.64). As usual MARE is a measure of the errors on the magnitudes of the two stars while RMSE is a measure of the error on the reconstructed PSF.

		300 it	500 it	2000 it
12-12 19 pixels	MARE	$8.78 \times 10^{-5}$	$4.35 \times 10^{-4}$	$4.49 \times 10^{-4}$
	RMSE	2.1 %	2.0 %	2.0 %
12-16 19 pixels	MARE	$4.72 \times 10^{-4}$	$3.21 \times 10^{-3}$	$1.62 \times 10^{-1}$
	RMSE	2.0 %	2.1 %	4.0 %
12-12 10 pixels	MARE	$4.36 \times 10^{-4}$	$2.28 \times 10^{-4}$	$4.36 \times 10^{-4}$
	RMSE	2.4 %	2.0 %	2.0 %
12-16 10 pixels	MARE	$1.99 \times 10^{-2}$	$5.91 \times 10^{-2}$	—
	RMSE	2.4 %	3.5 %	4.0 %

binary 12-12 and SR=0.67, we also consider the cases SR=0.4, 0.6, 0.8 and 1. The error on the PSF is of the order of 22 % in the case SR=0.4, about 5 % in the case SR=0.6 and about 11 % in the two other cases. We can add that the artifacts disappear in the case of underestimated SR. In conclusion an underestimate of SR of about 10 % (which does not correspond to the precision achievable in the experimental estimation of this parameter) is still acceptable, while an overestimate can be dangerous in all cases.

#### 4.4. Complex and diffuse objects

As additional examples of astronomical targets, we consider three HST images: the Crab nebula NGC 1952, the galaxy NGC 6946 and the planetary nebula NGC 7027. In all cases we assume an integrated magnitude equal to 10 and, for each one, we obtain three blurred images by convolving with the three PSFs of SR=0.67, 0.40 and 0.17. Again a background in H-band is added to all images and the results are perturbed with Poisson and additive Gaussian noise. In the first column of Fig. 4 we show the three objects in reversed scale of gray levels while in the second column we show their blurred images in the case SR=0.67.

As concerns the initialization of the blind algorithm we use the same PSFs already used in the case of stellar objects, namely obtained by suitable autocorrelations of the ideal PSF of the telescope. However in the case of complex and diffuse objects, as already remarked by other authors (see, for instance, [10]), a difficult and crucial point is the choice of the number of inner iterations. We do not have a rule which can be successfully applied to all cases as for the stellar objects, i.e.  $(n_f, n_h) = (50, 1)$ . By several attempts we find “best” numbers for each case, but it is obvious that this is not a satisfactory

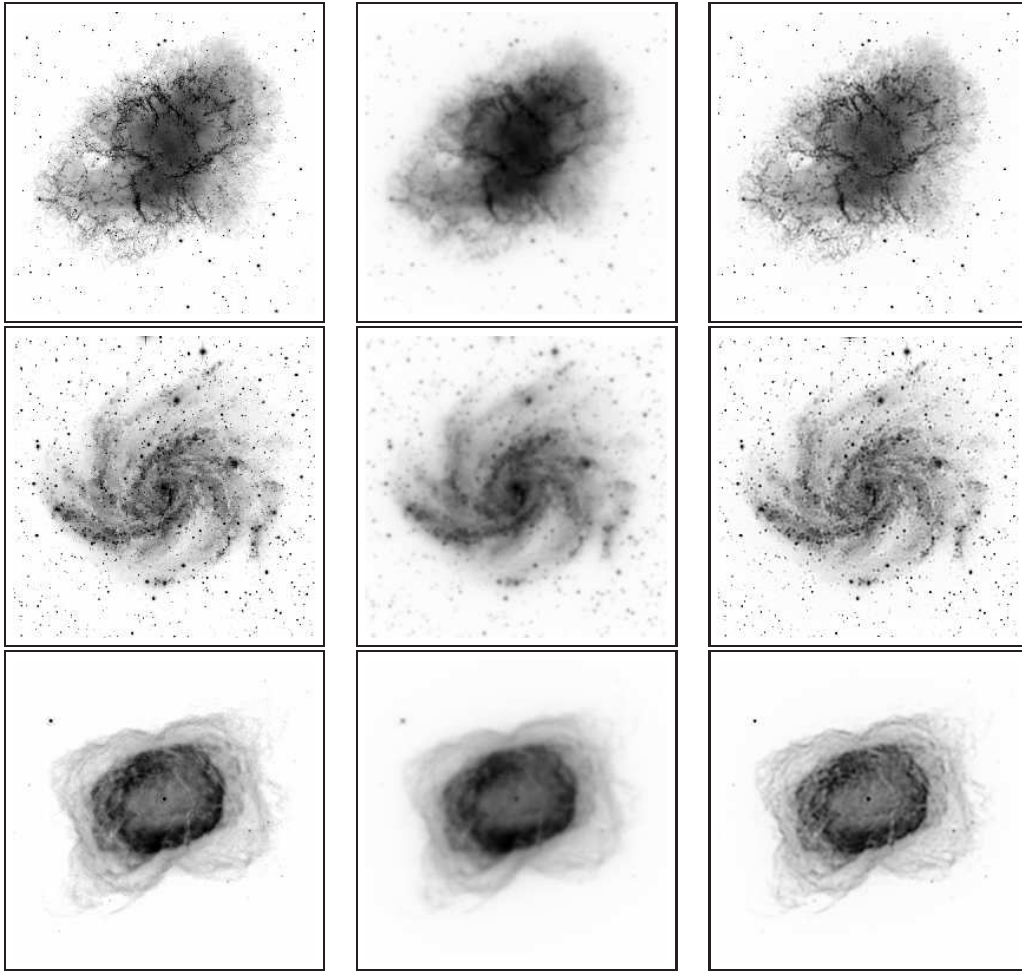
**Table 4.** Reconstruction errors for complex and diffuse objects. In third and fourth columns, the best errors achieved by SGP with the true and the initial PSFs, respectively. In the fifth column, the best error obtained using a maximum of 100 outer iterations (for the choice of the inner iterations see the text). Finally, in the last two columns, the error between the true PSF and the initial one, followed by the error between the true PSF and the one obtained in conjunction with the best reconstruction of the corresponding object.

Image	SR	$RMSE^{obj}$	$RMSE_1^{obj}$	$RMSE_2^{obj}$	$RMSE_1^{psf}$	$RMSE_2^{psf}$
Crab	0.67	11 %	16 %	12 %	32 %	6.7 %
	0.40	12 %	20 %	14 %	54 %	12 %
	0.17	15 %	22 %	16 %	55 %	16 %
Galaxy	0.67	14 %	23 %	16 %	32 %	7.4 %
	0.40	16 %	30 %	19 %	54 %	16 %
	0.17	20 %	35 %	23 %	55 %	21 %
Nebula	0.67	3.2 %	6.8 %	6.8 %	32 %	32 %
	0.40	3.5 %	8.9 %	8.9 %	54 %	53 %
	0.17	4.2 %	9.0 %	7.9 %	55 %	43 %

situation. For instance, in the case of the Crab nebula we find  $(n_f, n_h) = (13, 22)$  for  $SR=0.67$  and  $(n_f, n_h) = (13, 27)$  for  $SR=0.40$ , if we search for minimum RMSE on the object using 100 outer iterations. Moreover, even if the algorithm is convergent, the limit is not, in general, a sensible solution: a suitable stopping of the outer iterations is required. In other words the algorithm is semi-convergent [34, 4] as concerns the outer iterations, i.e. the RMSE on the object first decreases, reaches a minimum and then goes away. We do not have a proof of this feature which derives from the numerical experiments. It is obvious that such a situation is not satisfactory and we briefly discuss this point in the next section (see also the Introduction).

In Table 4 we report the best results we have obtained while in the third column of Fig. 4 we show the reconstructions of the objects provided by the blind algorithm. We stress the case of the planetary nebula: it seems that in this case the algorithm is unable to improve the reconstruction with respect to that provided by the initial guess. We also remark that the error on the reconstructed PSF depends on the object: for instance, for the galaxy it is larger than that for the Crab.

We conclude by reporting an experiment intended to check the effect of an underestimated or overestimated SR in the reconstruction of a diffuse object. We consider the case of the Crab nebula and PSF with  $SR=0.67$ , and we apply our algorithm with  $SR=0.6$  and  $SR=0.8$ . In the first case, the minimum RMSE on the object and the PSF are equal to 13% and 8.2%, while in the other the errors on object and PSF are 12% and 6.7%,



**Figure 4.** First column: the objects used for image generation; second column: the blurred images in the case of  $SR=0.67$ ; third column the reconstructed objects obtained with our blind algorithm. First row: the Crab nebula NGC 1952, second row: the spiral galaxy NGC 6946, third row: the planetary nebula NGC 7027.

which are essentially the same values obtained with the correct SR. The small variance observed suggests that, in presence of complex objects, the availability of a correct SR does not represent a crucial point. In this case, an overestimate of the SR value seems to be preferable.

## 5. Concluding remarks and perspectives

In this paper we propose a blind algorithm, based on SGP, for the reconstruction of astronomical images acquired by a telescope equipped with an AO system. The algorithm can be classified as an inexact alternating minimization of the KL divergence depending on

both the object and the PSF. The crucial point is the introduction of different constraints on the object and PSF and this can be done in a correct way by using the particular structure of SGP. Moreover the convergence of the algorithm is derived from general results proved in [14] on the convergence of inexact AM.

Since the problem is non-convex, the limit points of the sequence of iterates may depend on several parameters and, more specifically, on the initialization of the outer iterations and on the numbers of inner iterations. In the case of stellar (point-wise) objects we have rules for the initialization and the numbers of inner iterations which seem to be suitable for all cases we have considered. Obviously, the effectiveness of the approach must be tested by application to a much broader set of simulated images in a wide program of simulations (see, for instance, Chap. 12 of [4]) as well as to real images. We also observe that our blind approach can be possibly used in conjunction with specific codes, such as the so-called *StarFinder* [22], developed for accurate photometric and astrometric analysis of star clusters. These codes contain a method for extracting the PSF from the image of the star field; this PSF can be compared with and/or replaced by that provided by our blind approach; also in this case the analysis of simulated star fields, in particular crowded star fields, can help to understand when the blind approach is required.

As already remarked in the Introduction, the situation is not so clear in the case of more complex astronomical targets. Our preliminary simulations indicate that the proposed blind method has the semi-convergent property as concerns the outer iterations (the numbers of the inner iterations are fixed by the user and, in any case, they should not be too large). The difficulties found in optimizing the numbers of inner iterations may reside in the fact that in this paper we do not introduce regularization in the objective function. Due to the flexibility of SGP the method can be easily generalized to differentiable regularizers (one only needs to compute the gradient of the penalty and its positive part) and this generalization will be the subject of future work. We stress again that the crucial point is to identify regularizers which are suitable for specific classes of astronomical targets as well as regularizers which are suitable for AO corrected PSFs.

The codes of the algorithms presented and used in this paper are available under request.

## Acknowledgments

This work has been partially supported by MIUR (Italian Ministry for University and Research), PRIN2008 “Optimization Methods and Software for Inverse Problems”, grant 2008T5KA4L, and FIRB - Futuro in Ricerca 2012 “Learning meets time: a new computational approach for learning in dynamic systems”, contract RBFR12M3AC\_002, and by INAF (National Institute for Astrophysics) under the contract TECNO-INAf 2010 “Exploiting the adaptive power: a dedicated free software to optimize and maximize

the scientific output of images from present and future adaptive optics facilities". The Italian GNCS - INdAM (Gruppo Nazionale per il Calcolo Scientifico - Istituto Nazionale di Alta Matematica) is also acknowledged.

## References

- [1] Barrett H H and Meyers K J 2003 *Foundations of Image Science* (New York: Wiley and Sons)
- [2] Barzilai J and Borwein J M 1988 Two point step size gradient methods *IMA J. Numer. Anal.* **8** 141–8
- [3] Benvenuto F, Zanella R, Zanni L and Bertero M 2010 Nonnegative least-squares image deblurring: improved gradient projection approaches *Inverse Problems* **26** 025004
- [4] Bertero M and Boccacci P 1998 *Introduction to Inverse Problems in Imaging* (Bristol: IoP Publishing)
- [5] Bertero M, Bindi D, Boccacci P, Cattaneo M, EVA C and Lanza 1998 A novel blind deconvolution method with an application to seismology *Inverse Problems* **14** 815–33
- [6] Bertero M, Boccacci P, Desiderà G and Vicidomini G 2009 Image deblurring with Poisson data: from cells to galaxies *Inverse Problems* **25** 123006
- [7] Bertero M, Boccacci P, La Camera A, Olivieri C and Carbillat M 2011 Imaging with LINC-NIRVANA the Fizeau interferometer of the Large Binocular Telescope; state of the art and open problems *Inverse Problems* **27** 113001
- [8] Bertsekas D P 1999 *Nonlinear Programming* (Belmont: Athena Scientific)
- [9] Bertsekas D P and Tsitsiklis J 1988 *Parallel and Distributed Computation: Numerical Methods* (Belmont: Prentice-Hall)
- [10] Biggs D S C and Andrews M 1998 Asymmetric iterative blind deconvolution of multi-frame images *Proc. SPIE* **3461** 328–38
- [11] Bonettini S, Zanella R and Zanni L 2009 A scaled gradient projection method for constrained image deblurring *Inverse Problems* **25** 015002
- [12] Bonettini S and Prato M 2010 Nonnegative image reconstruction from sparse Fourier data: a new deconvolution algorithm *Inverse Problems* **26** 095001
- [13] Bonettini s and Ruggiero V 2011 An alternating extragradient method for total variation-based image reconstruction from Poisson data *Inverse Problems* **27** 095001
- [14] Bonettini S 2011 Inexact block coordinate descent methods with application to the nonnegative matrix factorization *IMA J. Numer. Anal.* **31** 1431–52
- [15] Carbillat M, Vérinaud C, Femenía B, Riccardi A and Fini L 2004 Modeling astronomical adaptive optics - I. The software package CAOS *Mon. Not. R. Astron. Soc.* **356** 1263–75
- [16] Chan T F and Wong C K 2000 Convergence of the alternating minimization algorithm for blind deconvolution *Linear Algebra Appl.* **316** 259–85
- [17] Dai Y H and Fletcher R 2006 On the asymptotic behaviour of some new gradient methods *Math. Program.* **103** 541–59
- [18] Dai Y H and Fletcher R 2006 New algorithms for singly linearly constrained quadratic programming problems subject to lower and upper bounds *Math. Program.* **106** 403–21
- [19] Dai Y H, Hager W W, Schittkowski K and Zhang H 2006 The cyclic Barzilai–Borwein method for unconstrained optimization *IMA J. Numer. Anal.* **26** 604–27
- [20] Desiderà G, Anconelli B, Bertero M, Boccacci P and Carbillat M 2006 Application of iterative blind deconvolution to the reconstruction of LBT LINC–NIRVANA images *Astron. Astrophys.* **452** 727–34

- [21] Desiderà G and Carillet M 2009 Strehl-constrained iterative blind deconvolution for post-adaptive-optics data *Astron. Astrophys.* **507** 1759-62
- [22] Diolaiti E, Bendinelli O, Bonaccini D, Close L M, Currie D G and Parmeggiani G 2000 StarFinder: an IDL GUI based code to analyze crowded fields with isoplanatic correcting PSF fitting *Proc. SPIE* **4007** 879-88
- [23] Fish D A, Brinicombe A M and Pike E R 1995 Blind deconvolution by means of the Richardson-Lucy algorithm *J. Opt. Soc. Am.* **A-12** 58-65
- [24] Frassoldati G, Zanghirati G and Zanni L 2008 New adaptive stepsize selections in gradient methods *J. Ind. Manag. Optim.* **4** 299-312
- [25] Grippo L and Sciandrone M 1999 Globally convergent block-coordinate techniques for unconstrained optimization *Optim. Method Softw.* **10** 587-637
- [26] Grippo L and Sciandrone M 2000 On the convergence of the block nonlinear Gauss-Seidel method under convex constraints *Oper. Res. Lett.* **26** 127-36
- [27] Hansen P C, Nagy J C and O'Leary D P 2006 *Deblurring Images. Matrices, Spectra, and Filtering* (Philadelphia: SIAM)
- [28] Holmes T J 1992 Blind deconvolution of quantum-limited incoherent imagery: maximum-likelihood approach *J. Opt. Soc. Am.* **A-9** 1052-61
- [29] Jefferies S M and Christou J C 1993 Restoration of astronomical images by iterative blind deconvolution *Astrophys. J.* **415** 862-74
- [30] Lantéri H, Aime C, Beaumont H and Gaucherel P 1994 Blind deconvolution using the Richardson-Lucy algorithm *Proc. SPIE* **2312** 182-92
- [31] Lee D D and Seung H S 2001 Algorithms for non-negative matrix factorization *Advances in Neural Information Processing 13 (Proc. NIPS\* 2000)* (MIT Press) 556-62
- [32] Levin A, Weiss Y, Durand F and Freeman W T 2009 Understanding and evaluating blind deconvolution algorithms *IEEE Conf. Computer Vision and Pattern Recognition* 1964-71
- [33] Luo Z-Q and Tseng P 1992 On the convergence of the coordinate descent method for convex differentiable minimization *J. Optimiz. Theory App.* **72** 7-35
- [34] Natterer F and Wübbeling F 2001 *Mathematical Methods in Image Reconstruction* (Philadelphia: SIAM)
- [35] Nocedal J and Wright S J 2006 *Numerical Optimization: Second Edition* (New York: Springer)
- [36] Powell M J D 1973 On search directions for minimization algorithms *Math. Program.* **4** 193-201
- [37] Prato M, Cavicchioli R, Zanni L, Boccacci P and Bertero M 2012 Efficient deconvolution methods for astronomical imaging: algorithms and IDL-GPU codes *Astron. Astrophys.* **539** A133
- [38] Snyder D L, Hammoud A M and White R L 1993 Image recovery from data acquired with a charge-coupled-device camera *J. Opt. Soc. Am.* **A-10** 1014-23
- [39] Snyder D L, Helstrom C W, Lanterman A D, Faisal M and White R L 1995 Compensation for readout noise in ccd images *J. Opt. Soc. Am.* **A-12** 272-83
- [40] Staglianò, Boccacci P and Bertero M 2011 Analysis of an approximate model for Poisson data reconstruction and a related discrepancy principle *Inverse Problems* **27** 125003
- [41] Tseng P 1991 Decomposition algorithm for convex differentiable minimization *J. Optimiz. Theory App.* **70** 109-35
- [42] Tsumuraya F, Miura N and Baba N 1994 Iterative blind deconvolution method using Lucy's algorithm *Astron. Astrophys.* **282** 699-708
- [43] Zanella R, Boccacci P, Zanni L and Bertero M 2009 Efficient gradient projection methods for edge-preserving removal of Poisson noise *Inverse Problems* **25** 045010
- [44] Zhou B, Gao L and Dai Y H 2006 Gradient methods with adaptive step-sizes *Comput. Optim. Appl.* **35** 69-86